SOLAR-WIND ION-DRIVEN X-RAY EMISSION FROM COMETARY AND PLANETARY ATMOSPHERES: MEASUREMENTS AND THEORETICAL PREDICTIONS OF CHARGE-EXCHANGE CROSS-SECTIONS AND EMISSION SPECTRA FOR O^{6+} + H_2O, CO, CO_2, CH_4, N_2, NO, N_2O, AND Ar

J. R. MACHACEK[1], D. P. MAHAPATRA[2], D. R. SCHULTZ[3], YU. RALCHENKO[4], A. MORADMAND[5], M. O. A. EL GHAZALY[5], AND A. CHUTJIAN[5]

[1] Atomic and Molecular Physics Laboratory, Research School of Physics and Engineering, The Australian National University, Canberra 2601, Australia
[2] Department of Physics, Utkal University, Bhubaneswar 751004, India
[3] Department of Physics, Univ. of North Texas, Denton, TX 76203, USA
[4] Atomic Spectroscopy Group, National Institute of Standards and Technology, Gaithersburg, MD 20899-8422, USA
[5] Astrophysics and Space Sciences Section, Jet Propulsion Laboratory/Caltech, Pasadena, CA 91109, USA

ABSTRACT

Relevant to modeling and understanding X-ray emission from cometary and planetary atmospheres, total cross-sections for 1.17 and 2.33 keV/u O^{6+} colliding with H_2O, CO, CO_2, CH_4, N_2, NO, N_2O, and Ar have been measured for the processes of single, double, and triple charge exchanges. Using these measurements as benchmarks, synthetic emission spectra spanning the X-ray, UV, and visible range have been calculated based on theoretical treatment of the transfer of between one and six electrons from the target neutrals to the projectile ion, followed by radiative and non-radiative decay of the highly excited states produced in these collisions. The results help add to the base of knowledge required to simulate ion-neutral processes in astrophysical environments; refine the present understanding of these fundamental atomic processes; and guide future observations, laboratory measurements, and theoretical predictions.

Key words: atomic processes – comets: general – molecular processes – solar wind

1. INTRODUCTION

Among the various mechanisms of X-ray emission in astrophysical environments, such as bremsstrahlung and synchrotron radiation, ubiquitous within the solar system is the resulting emission following the pickup of an electron from a neutral atom or molecule by a highly charged ion (HCI). In such charge exchanges (CEs) an HCI in (for example) the solar wind (SW) captures an electron from the neutral gas into a state with a high principal quantum number n that subsequently de-excites by emitting one or more photons at visible-to-X-ray wavelengths. Such emission occurs during the interaction of the SW with cometary atmospheres (Lisse et al. 1996; Cravens 1997; Krasnopolsky 1997; Ewing et al. 2013), with the atmospheres of Venus (Dennerl et al. 2002) and Mars (Dennerl et al. 2006), and in the Earth's geocorona, contributing to the pervasive soft X-ray background (Cravens et al. 2001; Collier et al. 2014; Wargelin et al. 2014). Emissions also occur at Jupiter, where not only SW ions but HCIs in the Jovian magnetosphere precipitate into the atmosphere to produce polar X-ray auroras (Cravens et al. 1995; Waite et al. 1997a, 1997b; Kharchenko et al. 2006; Hui et al. 2009). This ion precipitation participates in the coupling of the ionosphere and magnetosphere to the lower planetary atmosphere (Cravens et al. 2003; Ozak et al. 2013).

Understanding the origin of these emissions and simulating them allows one to extract astrophysical information such as neutral and ion composition, transport mechanisms, and the properties of neutrals and ions within the environment, and to understand the mechanisms that contribute to X-ray backgrounds. As such, one requires detailed knowledge of the CE process for the relevant ion-neutral collisions. In the present work, we seek to extend this knowledge for the most-abundant SW heavy ion O^{6+} (Schwadron & Cravens 2000), in collisions with the abundant cometary and planetary species (or their

atom-analog, here Ar). These targets are H_2O, CO, CO_2, CH_4, N_2, NO, N_2O, and Ar. Measurements and calculations of CE cross-sections for $^{18}O^{6+}$ + H_2 and He (Machacek et al. 2014) have recently been reported at two ion energies 1.17 keV/u (3.5 keV•q) and 2.33 keV/u (7.0 keV•q) (ion charge is $q = 6$), representative of the slow and fast components of the SW. Experimental X-ray spectra have also been reported for $^{16}O^{6+}$ + CO collisions at 36 keV ion energy (Miller et al. 2011).

The study of CE in ion-neutral collision studies has been ongoing for many decades. However, after the discovery of X-ray emissions in the solar system driven by ion impact, a number of studies have sought to either (i) provide directly relevant data for total cross-sections and spectra, or (ii) obtain a new physical understanding of the mechanisms underlying CE, such as the role of multi-electron processes as they pertain particularly to astrophysically relevant interactions. Noting a few of the many works carried out for ions at SW velocities, Beiersdorfer et al. (2001) measured and simulated X-ray emission following CE in O^{7+}, O^{8+} + CO_2 and Ne^{9+}, and Ne^{10+} + Ne. Hasan et al. (2001) provided experimental and theoretical results for N^{7+} and O^{7+} projectile ions colliding with He, H_2O, CO_2, and C. Mawhorter et al. (2007) reported measurements of single- and multiple-CE cross-sections for C, N, and O ions colliding with He, H_2O, CO, and CO_2, as well as single-capture (SC) cross-sections for He^{2+} on He and H_2 (Mawhorter et al. 2011).

The present work provides new total cross-section measurements for single, double, and triple CEs and benchmarks the present theoretical calculations of the state-selective, single-, double-, triple-, . . . 6-fold electron capture. Such high-multiplicity CEs result in both photon emission and auto-ionization (a non-radiative emission of one or more electrons). This necessitates a theoretical treatment of not only the electron

capture events, but also the subsequent radiative and non-radiative decays in order to predict total and state-selective capture cross-sections and emission spectra. The results allow important conclusions to be drawn regarding the role of multiple-electron exchanges, the variation of emission spectra for different molecular targets, and future directions of experimental and theoretical study to improve the reliability of the simulated spectra.

2. EXPERIMENTAL APPROACH

The experimental methods used herein parallel the procedures detailed in Machacek et al. (2014). Mass-selected $^{18}O^{6+}$ ions are produced in the Jet Propulsion Laboratory (JPL) electron cyclotron resonance ion source and extracted at potentials of $V_o = 3.5\,kV$ ("slow" SW) or $V_o = 7.0\,kV$ ("fast" SW). The O^{6+} ions are momentum-analyzed and electrostatically deflected through $45°$, then focused and collimated by an einzel lens system and a series of three apertures prior to entering the target gas cell. The ions undergo CE collisions in the cell to produce lower charge states by one, two, or three (or more) CEs. Ion currents for each CE step are measured using a retarding-potential analyzer placed at the end of the CE cell, and followed by a deep Faraday beam trap. A capacitance manometer is used to measure the target gas-cell pressure.

The currents in each charge state are measured through the sequential application of retarding potentials V_q, the values of which depend on the incident charge state q, and ion energy qV_o through the usual expression $V_q = qV_o/(q - j)$, where j is the number of exchanges. Thus a series of retardations V_1, V_2, V_3 and V_4 will block the charge states $q, q - 1, q - 2$, and $q - 3$, for a total of three exchanges, the maximum encountered in the present study.

As in Machacek et al. (2014), the cross-section $\sigma_{q,q-n}$ for the exchange of n electrons is given in terms of the experimentally measured parameters as

$$\sigma_{q,q-n} = \frac{kT}{PL} \ln\left(\frac{1}{1 - R_{q,q-n}}\right). \qquad (1)$$

Here, T is the target gas temperature, P is the gas pressure, L is the effective gas-cell length, and $R_{q,q-n}$ is the particles current ratio given by

$$R_{q,q-n} = \frac{qI_{q-n}}{(q - n)I_q}, \qquad (2)$$

where the currents $I_{q-1}, I_{q-2}, I_{q-3}$ and I_{q-4} correspond to measured currents in the steps after the application of the retarding potentials V_2, V_3 and V_4.

Additional details of the $^{18}O^{6+}$ mass/charge spectrometry, charge-state blocking voltages (including measurement of the background level), data acquisition, presence of metastable in the O^{6+} beam, tests for gas-cell pressure effects on CE cross-sections; together with sources and magnitudes of random and systematic errors are given in Machacek et al. (2014). The H_2O used in these studies was deionized grade, and subjected to five freeze-thaw cycles to eliminate dissolved gases.

3. THEORETICAL METHODS

Theoretical predictions complement and extend the utility of measurements by providing a means to test the physics underlying the experimental results, and upon validation they provide additional data where there are gaps, or where measuring was too difficult. In the present case, we seek to predict the quantity of the most use to astrophysical simulations and spacecraft observations, namely the absolute emission spectra. A complete theoretical approach for this would be to carry out fully quantum-mechanical calculations of both the multiple CEs that occurs in the collisions, and of the subsequent radiative and non-radiative rearrangement that occurs as the highly excited electronic state decays. However, for the first of these two steps, a fully quantum-mechanical treatment of multiple-electron capture by an HCI from a molecular target represents a significant challenge. Consequently, we adopt a more feasible approach in which the classical trajectory Monte Carlo (CTMC) method (Abrines & Percival 1966; Olson & Salop 1977; Olson et al. 1989) is used to simulate the ion-neutral collision that populates the electronic state following single- or multi-electron CE.

This approach is based on the solution of the classical equations of motion for a large ensemble of initial projectile-target configurations chosen to mimic the most important quantum-mechanical characteristics of the target, taking advantage of the fact that single and multiple CEs critically depend on the initial binding energies of the electrons in the neutral target. Upon calculation of each "trajectory" of this ensemble, the resulting events yield any one of the possible reactions including, for example, elastic scattering, target excitation, or transfer of one or more electrons to the projectile. This method has been used and benchmarked by measurements for collisions relevant to SW–cometary atmosphere interactions (Beiersdorfer et al. 2001), and in our previous work for the collision partners N^{7+}, O^{7+} + He, H_2O, CO_2, and CO (Hasan et al. 2001); Ne^{10+} + He, Ne, Ar, CO, and CO_2 (Ali et al. 2005); Ne^{10+} + He, Ne, and Ar (Ali et al. 2010); Fe^{q+} ($q = 5$–13) + H_2O (Simcic et al. 2010a), CO, and CO_2 (Simcic et al. 2010b); and O^{6+} + H_2 and He (Machacek et al. 2014). A description of the CTMC method can be found in these works and in the foundational papers (Abrines & Percival 1966; Olson & Salop 1977; Olson et al. 1989). As in the study of O^{6+} + H_2 and He (Machacek et al. 2014), we treat the two 1s electrons on the projectile as inactive and represent the target as containing six active electrons with the sequential binding energies for Ar, sourced from the National Institute of Standards and Technology (NIST) online atomic structure database (Kramida et al. 2014); and derived from the orbital binding energies for the molecular targets found from quantum-chemistry calculations tabulated in the NIST Chemistry WebBook (2015).

The CTMC simulation serves as an event generator, yielding a set of events in which one or more electrons, up to the six treated in the present model, are transferred to the projectile in the collisions that result in a CE. For each of these events, the principal (n) and angular momentum (ℓ) quantum numbers are calculated using correspondence rules (Becker & MacKellar 1983; Schultz et al. 2001). Each event represents an electronic state that may be stable or may decay via radiative or non-radiative transitions. Owing to the high initial charge of the projectile, the dominant principal quantum number to which CE proceeds is about $n = 4$ (with significantly more events with even higher n-levels), so the vast majority of the multiple capture decays via autoionization, a process typically much faster than radiative decay. In our previous work that sought only to determine the predicted single and multiple total CE

cross-sections, we used a simple model for the autoionization and radiative decay rates, and used transition propensities to model the subsequent decay sequence for multiple-capture events. Good agreement was found with the measurements of Fe^{q+} ($q = 5$–13) + H_2O (Simcic et al. 2010a), CO, and CO_2 (Simcic et al. 2010b).

More recently, in order to produce synthetic spectra of use in astrophysical modeling, we employed a combination of this decay simulation for 6-, 5-, 4-, and 3-fold capture events, and used an ab initio approach to process all the resulting direct double and SC events (Machacek et al. 2014). That is, owing to the challenge of using an ab initio atomic structure code to compute the energy levels, transition rates, and radiative–nonradiative branching ratios for up to six electron states in n-levels up to about 10, the simple model was used to reduce the difficulty of this task to the more feasible one including only doubly excited states. Here, to remove the uncertainty inherent to the use of the simple model for the higher-multiplicity, capture-event processing we have undertaken ab initio calculation of the atomic structure and decay parameters for up to four excited electrons above the $1s^2$ core of O^{6+}. This allows us to compare results of the simple model employed to process events all the way from 6-fold capture down to SC, with ab initio processing from fourfold capture to SC.

The basis of our previously employed ab initio processing is the use of a time-dependent collisional-radiative model (Ralchenko & Maron 2001) that takes into account radiative and autoionization processes describing the evolution of level populations after multi-electron CEs and resultant emission spectra. As noted, we previously applied this approach to the calculation of population stabilization following double CE in $O^{6+} + H_2$ and He, and found good agreement with the measured cross-sections. This method, however, becomes impractical for larger numbers of transferred electrons. When three or more electrons are captured into atomic shells with relatively high values of the principal quantum number and accordingly, $(n-1)$ values of the orbital angular momentum, the total number of possible combinations of the momenta is exceedingly large and thus the size of the rate matrix increases dramatically. For instance, the number of atomic levels with two electrons in the $n = 4$ shell only is 84, while for three electrons this grows to 678, and becomes 4430 for four N-shell electrons. For higher n-values, the number of states increases dramatically, as will be shown below. Therefore, other methods are required.

Here we implement a Monte Carlo (MC) approach to be described in detail elsewhere. In brief, CE events from the CTMC simulation are generated for $(n_1 \ell_1, n_2 \ell_2 ...)$ configurations of the final ion. Our MC model operates with relativistic configurations $(n_1 \ell_{1\pm}, n_2 \ell_{2\pm} ...)$ as calculated with the Flexible Atomic Code (FAC; Gu 2008). Thus the original CTMC-produced $n\ell$-states are split according to the statistical weights of the relativistic configurations. Although for single and double CEs available computational resources allow simulations in an even more detailed representation of atomic levels (i.e., fine structure components), for consistency, in the present work we make use of relativistic configurations for all ion charge states. The total numbers of such states for O^{5+} through O^{2+} are 99 ($n_{max} = 10$), 1896 ($n_{max} = 8$), 28,564 ($n_{max} = 7$),

Table 1
Comparison of the Present Measurements and Theoretically Predicted Single, Double, and Triple Charge-exchange Cross Sections

O^{6+} + Target, Energy, Channel	Present Measured Cross Section	Present Theoretical Cross Section	Ratio of Measurement to Theory
Ar 1.17 keV/u			
SCE	4.98 ± 0.34	5.90	0.84
DCE	0.84 ± 0.06	0.544	1.54
TCE	0.29 ± 0.02	0.0126	23.1
Ar 2.33 keV/u			
SCE	4.65 ± 0.31	6.32	0.74
DCE	0.71 ± 0.05	0.560	1.27
TCE	0.22 ± 0.02	0.0138	15.9
N_2 1.17 keV/u			
SCE	5.05 ± 0.34	3.76	1.34
DCE	0.96 ± 0.07	0.588	1.63
TCE	0.38 ± 0.03	0.0346	11.0
N_2 2.33 keV/u			
SCE	4.41 ± 0.30	4.04	1.09
DCE	0.74 ± 0.05	0.589	1.26
TCE	0.27 ± 0.02	0.0348	7.76
CO 1.17 keV/u			
SCE	5.41 ± 0.37	4.51	1.20
DCE	1.10 ± 0.08	0.579	1.90
TCE	0.37 ± 0.03	0.0477	7.76
CO 2.33 keV/u			
SCE	5.37 ± 0.37	4.78	1.12
DCE	0.79 ± 0.06	0.625	1.26
TCE	0.33 ± 0.03	0.0593	5.57
CH_4 1.17 keV/u			
SCE	4.29 ± 0.29	5.42	0.79
DCE	1.78 ± 0.13	0.676	2.63
TCE	0.27 ± 0.02	0.0659	4.10
CH_4 2.33 keV/u			
SCE	5.02 ± 0.34	5.67	0.89
DCE	1.63 ± 0.12	0.694	2.35
TCE	0.23 ± 0.02	0.0634	3.63
H_2O 1.17 keV/u			
SCE	4.73 ± 0.32	5.50	0.86
DCE	0.83 ± 0.06	0.630	1.32
TCE	0.37 ± 0.03	0.0580	6.38
H_2O 2.33 keV/u			
SCE	4.59 ± 0.31	5.74	0.80
DCE	0.74 ± 0.05	0.653	1.13
TCE	0.26 ± 0.02	0.0586	4.44
CO_2 1.17 keV/u			
SCE	4.40 ± 0.30	4.61	0.95
DCE	1.19 ± 0.09	0.659	1.81
TCE	0.52 ± 0.04	0.0632	8.23
CO_2 2.33 keV/u			
SCE	5.11 ± 0.35	4.89	1.05
DCE	1.20 ± 0.09	0.675	1.78
TCE	0.47 ± 0.04	0.0606	7.76

Table 1
(Continued)

O^{6+} + Target, Energy, Channel	Present Measured Cross Section	Present Theoretical Cross Section	Ratio of Measurement to Theory
N$_2$O 1.17 keV/u			
SC	4.38 ± 0.30	5.26	0.83
DC	1.21 ± 0.09	0.682	1.77
TC	0.36 ± 0.03	0.0651	5.53
N$_2$O 2.33 keV/u			
SCE	4.95 ± 0.34	5.50	0.90
DCE	1.23 ± 0.09	0.708	1.74
TCE	0.41 ± 0.03	0.0634	6.47
NO 1.17 keV/u			
SCE	5.24 ± 0.36	9.48	0.55
DCE	0.81 ± 0.06	0.622	1.30
TCE	0.29 ± 0.02	0.0627	4.63
NO 2.33 keV/u			
SCE	5.08 ± 0.35	9.66	0.53
DCE	0.73 ± 0.05	0.632	1.16
TCE	0.33 ± 0.03	0.0612	5.39
Average Over All Molecules 1.17 keV/u			
SCE	4.81 ± 0.84	5.6 ± 3.4	0.86 ± 0.54
DCE	1.09 ± 0.64	0.623 ± 0.10	1.8 ± 1.1
TCE	0.36 ± 0.16	0.0512 ± 0.038	7.0 ± 6.1
Average Over All Molecules 2.33 keV/u			
SCE	4.90 ± 0.64	5.8 ± 3.4	0.84 ± 0.50
DCE	0.97 ± 0.68	0.64 ± 0.10	1.5 ± 1.1
TCE	0.32 ± 0.18	0.0519 ± 0.036	6.2 ± 5.5

Note. Experimental values are cited at their 2σ level of uncertainty. Uncertainties in the averages of the measured and calculated cross-sections (last two rows) are given at the 2σ level, and the total error in the ratios are the individual 2σ errors added in quadrature. All cross-section units are 10^{-15} cm^2.

and 97,671 ($\ell_{max} = 7$), respectively. Note that the actual selection of atomic states is determined by the CTMC distribution of CE states and the ensuing decay channels. FAC is used to calculate all possible radiative and autoionization rates between these states.

The present implementation of the MC method is close to the "kinetic MC" approach (Kalos & Whitlock 2008; Son & Santra 2012). However, since the characteristic times τ of atomic processes ($\tau \lesssim 10^{-13}$ s for autoionization and $\tau \lesssim 10^{-9}$ s for radiative processes) are much smaller than the ion flight times between the gas cell and the detector $\tau_f \sim 10^{-6}$ s in the present experiment (and, of course, in the relatively low-density astrophysical environments to which it is relevant), we neglect any time dependence that is typical for kinetic MC calculations. This assumption, confirmed by test calculations, means that a complete stabilization of populations is achieved within τ_f.

The calculational procedure is as follows.

1. For each state j of an ion (having, say, N possible decay channels), all of its radiative and autoionization rates are normalized to the sum of all rates and sorted in decreasing order: $R_{i+1} \leqslant R_i$, $i = 1$ to N, and $\Sigma_i R_i = 1$.
2. A new recursive set of effective rates is generated via: $\rho_0 = 0$; $\rho_1 = R_1$; $\rho_{i+1} = \rho_i + R_{i+1}$ for $i > 1$; $\rho_N = 1$.
3. A random number is chosen, $r \in (0, 1]$. If $\rho_{i-1} < r \leqslant \rho_i$, the ith decay channel is selected and the procedure is repeated from step 1.
4. If the decay channel is radiative, the energy of the emitted photon is recorded.
5. The calculation stops when an ion ground state is reached.

In order to collect significant statistics, this procedure is repeated 10^6 times for each initial state. The calculation times are from two minutes for a double CE, to about 50 minutes for a quadruple CE on a typical workstation.

The result of the CTMC simulations, post-processed by either the simple model of the subsequent evolution of the excited, possibly multiple-electron events, or by the more ab initio approach, yields the single, double, etc., total cross-sections for comparison with the present measurements. The ab initio approach yields the predicted emission spectra.

4. RESULTS AND DISCUSSION

The results of the present measurements and calculations are given in Table 1, namely the total cross-sections for single, double, and triple CEs in 1.17 and 2.33 keV/u O^{6+} colliding with H$_2$O, CO, CO$_2$, CH$_4$, N$_2$, NO, N$_2$O, and Ar. Shown in the table is the ratio of the measurement to the theory for each target neutral, impact energy, and CE channel. Also shown are several statistical measures of the variation of the results and the deviation of the predictions from measurements.

It should be noted from Table 1 that the single CE cross-sections varies only slightly as the molecular target is changed. Specifically, the average measured SC cross-section for the molecular targets is $4.81 \pm 0.42 \times 10^{-15}$ cm^2 (for 1.17 keV/u), that is, showing only about a 9% variation as measured by the standard deviation. This is in general agreement with the present theoretical prediction of $5.6 \pm 1.7 \times 10^{-15}$ cm^2 for the same average. In fact, the average of the ratios of the individual measured and corresponding predicted SC cross-sections is 0.86 ± 0.27, showing that the theory closely agrees with the experiment when averaged over results for the molecular targets. These averages change by only about two percent at the higher impact energy.

The results are similar for the double capture (DC) total cross-section, with the average for the molecular targets being $1.09 \pm 0.32 \times 10^{-15}$ cm^2 from the measurements (at 1.17 keV/u), and $0.623 \pm 0.05 \times 10^{-15}$ cm^2 from theory. For DC, the corresponding average of the ratios of the measurements to the corresponding predictions is 1.8 ± 0.55, significantly larger than for SC capture, indicating an underestimate by a factor of 1.8 of the predicted total number of events in the simulation, that should result in a stable DC. Both these trends–relative equality of the measured cross-sections and a growing underestimation by theory–continue for triple capture (TC). Measured total cross-sections for TC vary by only 20% on average for the molecular targets (at 1.17 keV/u), but the predictions are on average about a factor of 7.0 too small.

The physical origin of this lack of strong variation of the total cross-sections for single, double, and triple CEs comes from the dominant dependence of the capture process on the initial binding energies of the electrons in the target. For
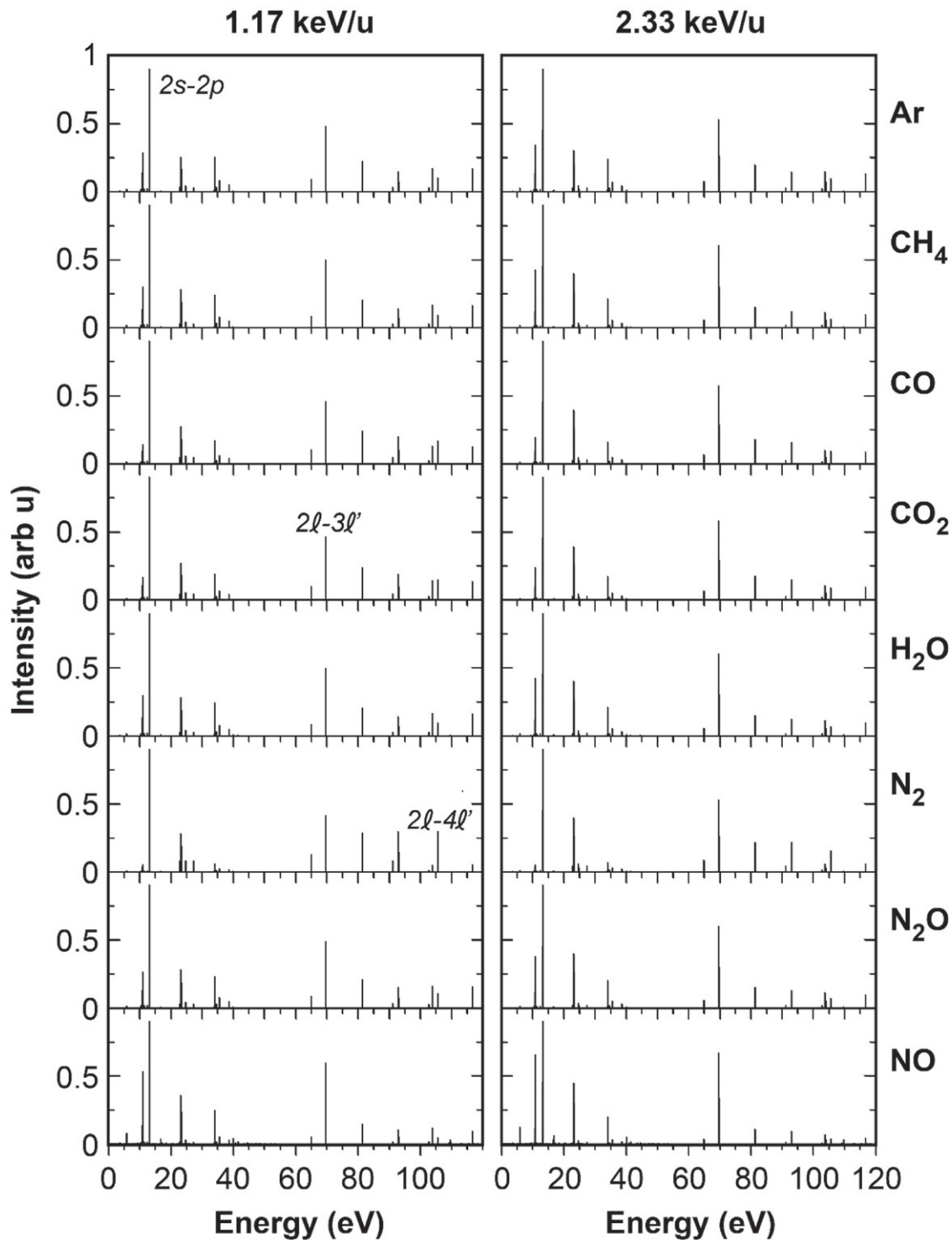
Figure 1. Emission spectra from single charge exchange of O^{6+} with the neutral targets, computed for the two collision energies, 1.17 and 2.33 keV/u.

example, the deviation from the average first ionization potential of the molecular targets is only 7%, and is 13%, 14%,17%, 16%, and 18% for the second, third, fourth, fifth, and sixth ionization potentials, respectively. Thus, because there is very little variation in the energy by which the first electron to be removed is bound among the molecules, the population—both in relative number and dominantly populated $n\ell$ levels—is similar for SC of O^{6+} colliding with any of these molecules. Similarly, since the second, third, etc., binding energies are similar for each molecule, the population of 2-electron, 3-electron, etc., states in both number and distribution in $n\ell$ is quite similar for all of the molecular targets, and therefore even after the non-radiative decay of multiple-electron capture states the resulting amounts of stable double electron capture, triple electron capture, etc., are quite similar. The same physical mechanisms indicate that the emission spectra should be quite similar for O^{6+} colliding with any of the molecules (as discussed below).
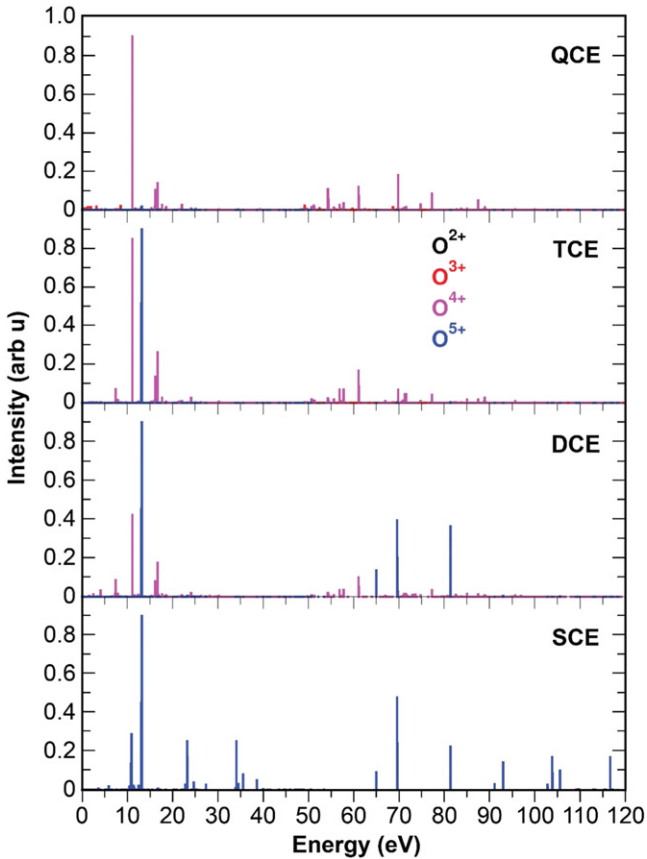
Figure 2. Emission spectra predicted for O^{6+} impact of Ar following single (SCE), double (DCE), triple (TCE), and quadruple (QCE) charge exchange. Emission from states of O^{5+} are displayed in blue, and those from O^{4+} are in pink, those from O^{3+} are in red, and those from O^{2+} are in black.

Beyond the dependence on electronic binding energy, which is the characteristic most reasonably modeled by the CTMC simulations, CE at relatively low collisions energies, such as those typical of the SW, depends quantum mechanically on the presence, position, and closeness of so-called quasi-molecular curve crossings. That is, in a fully quantum-mechanical approach, at low collision energy, the electronic state of the projectile plus target system evolves along quasi-molecular energy states (e.g., the eigenenergies of the $[ON_2O]^{6+}$ molecular ion for the case of O^{6+} colliding adiabatically with N_2O) and can make transition among them where these states become close in energy localized at certain internuclear separations. The uniformity of the measured cross-sections can be interpreted as indicating that none of these collision systems have a dramatically different dominant quasi-molecular curve crossing. Furthermore, the lack of significant variation in the measured cross-sections in the small range of energy change between 1.17 and 2.33 keV/u indicates there is no strong impact-energy dependence on the dominant quasi-molecular crossings. Both of these observations also tend to indicate that this is why the CTMC model, based most significantly upon correct quantum-mechanical binding energies rather than the quasi-molecular curve crossings, can do as good a job as it does in reproducing the measurements.

Regarding the behavior in which the CTMC approach does well reproducing the SC results, but increasingly underestimates higher-multiplicity capture, we found a way to improve this in our previous work considering single and double CEs in $O^{6+} + H_2$

and He (Machacek et al. 2014), because of the relatively simple electronic structure of those targets. That is, the CTMC approach in which the electronic binding energies are chosen to be the sequential ionization potentials has been shown to provide reliable results for HCI impact, for example, in ions with charge states $q \geqslant 20$. In such a case the great strength of the Coulomb interaction of the HCI with the neutral target pulls the electrons off in the collision and the total energy deposition, represented by the sum of the sequential ionization potentials, is the dominant determining factor in the cross-section for multiple CE (Olson et al. 1989). This is, therefore, the basis of the CTMC model that uses the sequential target electron binding energies, conventionally denoted as "nCTMC" ("n" simply for n electrons). In contrast, for low charge state projectile ions, consider for example the extreme case of proton impact or another singly charged ion, the target electrons interact with it more as if they were all bound by a common ionization potential, the so-called independent electron model (and quasi-molecular curve crossing effects could be large as well). A CTMC model with all of the electrons bound by the same potential within one electronic shell (the six 2p electrons in Ne, for example) is more appropriate in this case. We denote it as "inCTMC" ("in" for "independent electron model").

For the present O^{6+} case we have an intermediate charge, and some combination of nCTMC and inCTMC models may be more appropriate. For H_2 and He (Machacek et al. 2014) simple quantum-mechanical wavefunctions are readily available that decompose into correlated (i.e., taking electron–electron interaction into account and thus yielding sequential binding energies, as in nCTMC) and uncorrelated (with each electron bound by the same energy, as in inCTMC) portions. For the molecular targets herein, we do not have such a readily available analysis of the relative portion of correlated (nCTMC) and uncorrelated (inCTMC) models that should be used; nor is it apparent what the magnitude of the contributions to multiple CEs of quasi-molecular effects might be. Therefore, future work could attempt a hybrid nCTMC–inCTMC approach, as we successfully employed for $O^{6+} + H_2$ and He, or the much more challenging fully quantum-mechanical treatment of the CE process including multi-electron capture up to relatively high n-levels.

Further evidence supporting this interpretation, namely that the origin of the underestimation of the DC and TC cross-sections comes from too small of an initial population of multiple-capture states, is provided by a comparison of the results of the ab initio processing with the simple model that was employed in previous work. For both 1.17 and 2.33 keV/u impact energies, the ratio of the ab initio-processed results and the simple model of carrying out the post-collisional de-excitation is 1.01 ± 0.01. The deviation increases only slightly for DCs for which the ratio is 1.04 ± 0.05 (at 1.17 keV/u) and 1.09 ± 0.01 (at 2.33 keV/u). Even for TC the ratio of the ab initio to simple model results is 0.664 ± 0.069 (1.17 keV/u) and 0.688 ± 0.055 (2.33 keV/u). Therefore, the deviation of the double and triple CE cross-sections from the measured values is less strongly affected by improvement of the de-excitation processing of the multiple-capture events than by the size and composition of the multiple capture, multiply excited population seeded in the collision.

We also note that the present methods yield reasonable agreement for the SC and DC for the Ar target (the ratios of measurement to theory are 0.844 and 1.54, respectively), in line with that for the molecular targets, but that the TC cross-section is farther off (ratio of 23.3 for 1.17 keV/u and 16.0 for

2.33 keV/u). The origin of this greater deviation is not likely from a significant difference in the sequential ionization potentials for argon (1st IP 15.8 eV, 2nd 27.8 eV, 3rd 41.9 eV, 4th 59.9 eV, 5th 75.1 eV, and 6th 90.9 eV) compared to the molecules (e.g., for CO_2: 13.8, 28.8, 43.5, 58.5, 78.1, and 98.0 eV, respectively). The measured SC, DC, and TC cross-sections for Ar are nearly the same as for the molecules: for 1.17 keV/u, the Ar SC, DC, and TC cross-sections are 4.98, 0.84, and 0.29×10^{-15} cm^2 compared to the average for the molecular targets of 4.81, 1.09, and 0.36×10^{-15} cm^2. Because of this, Ar makes a reasonable "surrogate" for the range of molecular targets considered here (composed of H, C, N, and O).

Even given the underestimation of the DC and TC cross-sections by the present predictions, it is important to note the role that multiple capture plays in contributing to the process that results in stable multiple capture. For example, for a typical case of, say, $O^{6+} + CO$ at 1.17 keV/u, about 1/3 of the TC events come from autoionization of fourfold (or higher) multiple capture, with the other 2/3 being from direct TC. Furthermore, the TC events coming from the autoionization of high-multiplicity capture tend to be more stable than those from direct TC. That is, as each higher-multiplicity capture event autoionizes, one electron is ejected into the continuum and the other drops to a lower principal quantum number (dominantly $\Delta n = 1$), thus increasing the stability of the remaining multi-electron excited states. In contrast, TCs proceed mostly to states with the three electrons in very similar (if not the same) n-levels, and thus dominantly autoionize from TC to DC or ultimately SC. Therefore, the role of post-collisional de-excitation is very important to the production of stable electronic configurations, and thus to the magnitudes of the DC and TC cross-sections and the states from these configurations that subsequently emit photons via radiative decay.

For SC, the dominant contribution to the emission spectra comes from direct SC events. Again using $O^{6+} + CO$ at 1.17 keV/u as an example, about 85% of the SC events come from the direct capture of just one electron and the remaining 15% come from the autoionization of two-electron or higher-multiplicity events. Combining this observation that SC is dominantly dependent on direct SC (and thus not dependent on the model's underestimation of the higher-multiplicity capture or the radiative–non-radiative decay processing) and the good agreement with the measured SC cross-sections, the predicted emission spectra for SC (displayed in Figure 1) is likely reasonable. Previous favorable comparison with $n\ell$-resolved measured cross-sections for the targets H_2 and He (Machacek et al. 2014) strengthens this likelihood. However, an ultimate confirmation would come from new measurements of the $n\ell$-resolved cross-sections or the multi-waveband spectra for one or more of the presently considered molecular targets. As noted above based on our predicted results, the general similarity of the spectral patterns is due to only minor differences in the distribution of the populated states. This would likely complicate the identification of neutrals due to single CEs alone for O^{6+} impact. Nonetheless, some peculiarities can be identified. For example, single CE with N_2 results in strong $n = 4 - 2$ transitions near 100 eV, while NO produces rather strong $5 - 4$ transition lines at $\sim$11 eV. The predicted emission spectra associated with DC, TC, and QC (see Figure 2 for $O^{6+} + Ar$ at 1.17 keV/u) are illustrative of the different $n\ell$ distributions populated directly and via non-radiative decay in

multiple CE. They are successively less reliable owing to the underestimation by the present model and the lack of confirming measurements, but nevertheless provide estimates for the emission from these channels.

5. CONCLUSIONS

We have reported measured single, double, and triple CE total cross-sections for O^{6+} colliding with H_2O, CO, CO_2, CH_4, N_2, NO, N_2O, and Ar at energies typical of the fast and slow SW relevant to X-ray emission from cometary and planetary atmospheres. In addition, we have provided theoretical predictions of these cross-sections based on nCTMC simulations of the collisions and ab initio radiative–non-radiative modeling of the decay of the excited product states to predict the emission spectra and test the results through comparison with the measured total cross-sections.

An important conclusion is that for this regime of impact energy, the total cross-sections and corresponding emission spectra vary slightly with target species, since the electronic binding energies are consistent for the molecular targets and Ar. We have also noted the importance of autoionization as a significant contributor to the stabilization of multiple capture. We have eliminated the uncertainty through the use of a simple model to treat this post-collisional de-excitation by introducing a new Monte Carlo approach based on ab initio atomic structure and radiative and non-radiative transition rates and branching ratios. A shortcoming of the collision simulation that populates the multiple electronic states has been noted, along with a possible origin of the discrepancy. The results add to the base of knowledge needed to model ion-neutral processes in astrophysical environments, contribute to the fundamental understanding of single and multiple CE processes, and indicate potential pathways for further improvement of theoretical predictions and needs for new measurements.

REFERENCES

Abrines, R., & Percival, I. C. 1966, PPSL, 88, 861
Ali, R., Neill, P. A., Beiersdorfer, P., et al. 2005, ApJL, 629, L125
Ali, R., Neill, P. A., Beiersdorfer, P., et al. 2010, ApJL, 716, L95
Becker, R. L., & MacKellar, A. D. 1983, JPhB, 17, 3923
Beiersdorfer, P., Lisse, C. M., Olson, R. E., Brown, G. V., & Chen, H. 2001, ApJL, 549, L147
Collier, M. R., Snowden, S. L., Sarantos, et al. 2014, JGR, 119, 1459
Cravens, T. E. 1997, GeoRL, 24, 105
Cravens, T. E., Howell, E., Waite, J. H., et al. 1995, JGR, 100, 17153
Cravens, T. E., Robertson, I. P., & Snowden, S. L. 2001, JGR, 106, 24883
Cravens, T. E., Waite, J. H., Gombosi, T. I., et al. 2003, JGR, 108, 1465
Dennerl, K., Burwitz, V., Englhauser, J., Lisse, C., & Wolk, S. 2002, A&A, 386, 319
Dennerl, K., Lisse, C. M., Bhardwaj, A., et al. 2006, A&A, 451, 709
Ewing, I., Christian, D. J., Bodewits, D., et al. 2013, ApJ, 763, 66
Gu, M. F. 2008, CaJPh, 86, 675
Hasan, A. A., Eissa, F., Ali, R., Schultz, D. R., & Stancil, P. C. 2001, ApJL, 560, L201
Hui, Y., Schultz, D. R., Kharchenko, V. A., et al. 2009, ApJL, 702, L158
Kalos, M. H., & Whitlock, P. A. 2008, Monte Carlo Methods (Weinheim: Wiley-VCH)
Kharchenko, V., Dalgarno, A., Schultz, D. R., & Stancil, P. C. 2006, GeoRL, 33, 11105

Kramida, A., Ralchenko, Yu., Reader, J. & NIST ASD Team 2014, NIST Atomic Spectra Database (version 5.2) (Gaithersburg, MD: National Institute of Standards and Technology)

Krasnopolsky, V. 1997, Icar, 128, 368

Lisse, C. M., Dennerl, K., Englhauser, J., et al. 1996, Sci, 274, 205

Machacek, J. R., Mahapatra, D. P., Schultz, D. R., et al. 2014, PhRvA, 90, 052708

Mawhorter, R. J., Chutjian, A., Cravens, T. E., et al. 2007, PhRvA, 75, 032704

Mawhorter, R. J., Greenwood, J. B., Chutjian, A., et al. 2011, PhRvA, 84, 052714

Miller, K. A., Smith, W. W., Ehrenreich, T., et al. 2011, ApJ, 742, 130

NIST Chemistry WebBook 2015, in NIST Standard Reference Database Number 69, ed. P. J. Linstrom & W. G. Mallard

Olson, R. E., & Salop, A. 1977, PhRvA, 16, 531

Olson, R. E., Ullrich, J., & Schmidt-Böcking, H. 1989, PhRvA, 39, 5572

Ozak, N., Cravens, T. E., & Schultz, D. R. 2013, GeoRL, 40, 4144

Ralchenko, Yu., & Maron, Y. 2001, JQSRT, 7, 1609

Schultz, D. R., Stancil, P. C., & Rakovic, M. J. 2001, JPhB, 34, 2739

Schwadron, N. A., & Cravens, T. E. 2000, ApJ, 544, 558

Simcic, J., Schultz, D. R., Mawhorter, R. J., et al. 2010a, ApJ, 722, 435

Simcic, J., Schultz, D. R., Mawhorter, R. J., et al. 2010b, PhRvA, 81, 062715

Son, S. K., & Santra, R. 2012, PhRvA, 85, 063415

Waite, J. H., Gladstone, G. R., Lewis, W. S., et al. 1997a, Sci, 276, 104

Waite, J. H., Lewis, W. S., Gladstone, G. R., et al. 1997b, AdSpR, 20, 243

Wargelin, B. J., Kornbleuth, M., Martin, P. L., & Juda, M. 2014, ApJ, 796, 28